ISIJ International, Vol. 38 (1998), No. 4, pp. 357–365

An Investigation of the Crystallization of a Continuous Casting Mold Slag Using the Single Hot Thermocouple Technique

Yoshiaki KASHIWAYA, Carlos E. CICUTTI[1] and Alan W. CRAMB[2]

Formerly Faculty of Engineering, Hokkaido University. Now at Department of Materials Science and Engineering, Carnegie Mellon University, Pittsburgh, PA, USA. 1) Formerly Department of Materials Science and Engineering, Carnegie Mellon University. Now at Center for Industrial Research, FUDETEC, Argentina. 2) Department of Materials Science and Engineering, Carnegie Mellon University, Pittsburgh, PA, USA.

(Received on October 6, 1997; accepted in final form on December 11, 1997)

The conditions under which crystallization develops in a mold slag must be understood in order to select or design a mold flux for use in the continuous casting of steels. In this paper, the crystallization of an industrial mold slag was quantified using a single hot thermocouple technique which, when combined with a video camera based observation system, allowed observation of the onset and growth of the crystals which were precipitated from the melt. The beginning of crystallization was determined by direct observation and the growth rate of crystals were measured by frame by frame image analysis of recordings of the progress of crystallization. Isothermal experiments were performed at different temperatures and a Time–Temperature-Transformation (TTT) diagram was determined for this industrial mold slag. X-ray diffraction of quenched samples was used to determine the type of crystalline phases that were precipitated. The TTT diagram was divided into two separate regions which corresponded to the precipitation of dicalcium silicate (Ca_2SiO_4) at temperatures over 1 050°C and of Cuspidine ($Ca_4Si_2O_7F_2$) at temperatures below 1 050°C. The evolution crystal fraction was described by Avrami's equation. This work indicates that industrial mold slags are easily undercooled, that crystallization occurs throughout the melt, that crystals grow initially as equiaxed dendrites and that the onset of crystallization is a function of cooling rate and must be described by either TTT or CCT curves.

KEY WORDS: mold flux; continuous casting; crystallization; nucleation; crystal growth; silicate; slag; hot thermocouple; TTT diagram.

1. Introduction

It is well known that mold slags* play a decisive role in lubrication and heat transfer control in the continuous casting mold[1] when steels are cast. Various studies [2,3] have shown that the slag film formed between mold and strand contains three layers: a glassy zone close to the mold, a crystalline layer in the center and a liquid film in contact with the steel. The proportion of crystalline and glassy phases in the slag film have been reported to help control the heat transfer rate in the mold[4–6]; however, as yet there has been no quantification of the specifics of mold slag crystallization or of the temporal development of the crystalline fraction. It is postulated that those slags which develop a crystalline layer at higher temperatures allow a reduction in the heat transfer rate between the mold and strand[7,8] and this design criteria has proved to be effective in the reduction of surface defects, mainly when peritectic steels are cast.[7,9,10] Slags with a high crystallization tendency are always used at lower cast speeds as these slags have been shown to increase the possibility of sticking type breakouts at higher cast speeds due to an increase in the friction between the mold and the strand.[11–13] Thus, the control of crystallization within a mold flux is a key parameter in the prudent operation of a steel continuous caster; however, as yet, the phenomena of crystallization of mold fluxes has been clearly described.

A variety of methods have been traditionally used to determine the crystallinity of mold slags; however, currently there is no standard technique for its evaluation.[14,15] **Table 1** summarizes a variety of methods reported by different authors in the literature. The most common method is Differential Thermal Analysis (DTA). In this case, the slag sample is melted in a furnace and then cooled simultaneously with a reference substance, and the temperature difference between both is recorded. When an endothermic or an exothermic reaction takes place in the sample, a temperature difference can be detected. The onset temperature of the exothermic peak

* Mold slags are the liquids that form upon the melting of the mold powders or mold fluxes that are added to the mold of a continuous caster used in the processing of liquid steel. The mold slag composition can be slightly different in composition from the mold powder or flux due to absorption of inclusions or reaction with the liquid steel.

Table 1. Methods and conditions employed for studying crystallization phenomena in mold slag.

Method employed	Cooling rate (°C/s)	Cooling rate (°C/min)	Reference
DTA	0.017	1	17)
DTA	0.17–33.3	10–2 000	18), 19)
DTA	0.42	25	20)
DTA	0.33	20	21)
DTA	0.17–1	10–60	22)
DTA (heating)	0.08–0.67	5–40	23)
DTA (heating)	0.17	10	24)
Cooling curve	~0.08	~5	8)
Hot microscope	0.33	20	12), 13)
Hot thermocouple	15	900	16), 13),
Casting in metallic mold			18), 22), 25)–28)

is usually called the "Crystallization Temperature" of the mold slag. Fundamentally the onset of crystallization must be a function of the cooling rate in these easily glass forming slags; however, as shown in Table 1, there is no unique criteria to define the cooling rate employed in the experiments. Several studies have considered the effect of cooling rate on the crystallization temperature[18,19–22] but only a few have attempted to construct Time Temperature Transformation (TTT) diagrams or Continuous Cooling Transformation (CCT) diagrams which would unambiguously describe the crystallization phenomena.

There have been numerous other techniques to determine crystallinity reported in the literature. For example, slag samples were first melted and rapidly cooled to room temperature in order to keep them in a glassy state.[23,24] After that, DTA analysis was performed during heating of the sample and the temperature at which crystallization appears was recorded. This kind of experiment is usually called a "Recrystallization test".

A slightly different method was applied by Kyoden *et al.*[8] to determine slag crystallinity. In this case, the slag sample was melted and then cooled down in a furnace. Temperature of the sample was recorded. When a deviation in the cooling curve was observed, it was attributed to the beginning of crystallization. Another method consisted of fusion of the slag sample in a high temperature microscope and observation of its behavior during cooling.[12,13,16] The temperature at which the slag lost transparency was considered to be the crystallization temperature.

Finally, a technique that was employed to better simulate a continuous casting mold consists of melting the mold slag sample, increasing its temperature to 1 550°C and then quenching it by pouring the molten slag into a metallic mold.[13,18,22,25–28] After that, the sample can be inspected, at room temperature, by a number of different techniques. For example, the proportion of crystalline and glassy phases can be evaluated using an optical microscope.[13,18,25,26] In other studies, the fracture surface of the slag was examined to estimate the percentage of crystallized area.[25] X-ray diffraction can also be performed to determine the structure and chemistry of the crystalline phases.[13,18] Obviously, these methods are useful to define a "crystallinity index" that can be used to compare, qualitatively, the tendency of different slags to give glassy or crystalline phases. However, they do not provide a quantitative measurement that can characterize the slag behavior in the mold.

In actual continuous casting operation, once the mold powder is melted on the top of the liquid steel and the liquid slag infiltrates between the mold and the strand surface, the liquid slag is exposed to different cooling paths which can promote or prevent crystallization. In fact it is common to see glassy parts of the slag in areas of high cooling rates with crystalline fractions at lower cooling rates. So, a proper characterization of the mold powder should include a complete description of the transformation kinetics. As mentioned before, some studies have shown the effect of the cooling rate on the crystallization temperature of mold powders.[18,19,22] However, few attempts have been made to develop a TTT curve, which provides a more fundamental understanding of the transformation process. Therefore, the main objective of this work was to develop a technique which would unambiguously allow the determination of a TTT curve for an industrial mold powder.

In a previous study,[29] the double and single hot thermocouple techniques (DHTT and SHTT) were developed and the details of temperature measurement and *in situ* observation were shown. The main advantage of these techniques are that crystallization occurring in the sample can be observed *in situ* under defined thermal conditions and the growth rate of crystals and the changes in the crystallized fraction can be measured. Also, due to the low thermal inertia of the system, high heating and cooling rates can be easily obtained. This is very useful for the determination of TTT diagrams where a fast initial cooling rate is required.

2. Experimental

Experiments were carried out using a single hot thermocouple technique (SHTT) and the details of the experimental apparatus were shown in a previous paper.[29] A slag sample was mounted on a Pt–Rh thermocouple (B Type) which was heated directly while its temperature was measured simultaneously. The thermocouple was located below a microscope equipped with a video camera, which sent the image to a computer and a VCR (Video Cassette Recorder). Heating and cooling of the thermocouple was controlled by means of a computer program so that different thermal cycles could be imposed.

Experiments were carried out using an industrial mold slag whose characteristics are shown in **Table 2**. It is a commercial mold powder normally employed in the continuous casting of stainless steels. In this case, the powder was prepared by the supplier without carbon in order to facilitate the experiments.

Figure 1 shows the typical thermal cycle employed in this study. First of all, a small sample (10 mg) of mold powder was melted on the tip of thermocouple. In all

Table 2. Chemical composition and physical properties of industrial mold slag.

Chemical composition (mass%)								Basicity CaO/SiO_2	Viscosity at 1 300°C (Pa·s)
T.CaO	SiO_2	Al_2O_3	Na_2O	T.F	MgO	K_2O	Fe_2O_3		
37.8	33.3	7.9	8.2	8.4	0.6	0.6	1.7	1.14	0.2

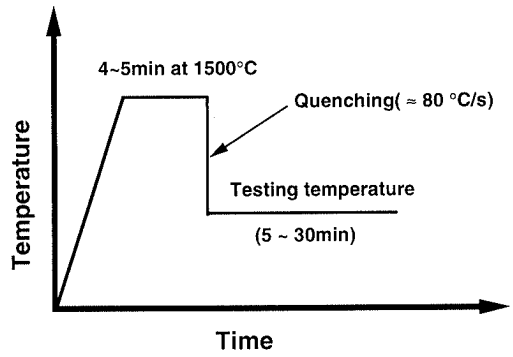

Fig. 1. Thermal cycle of experiment.

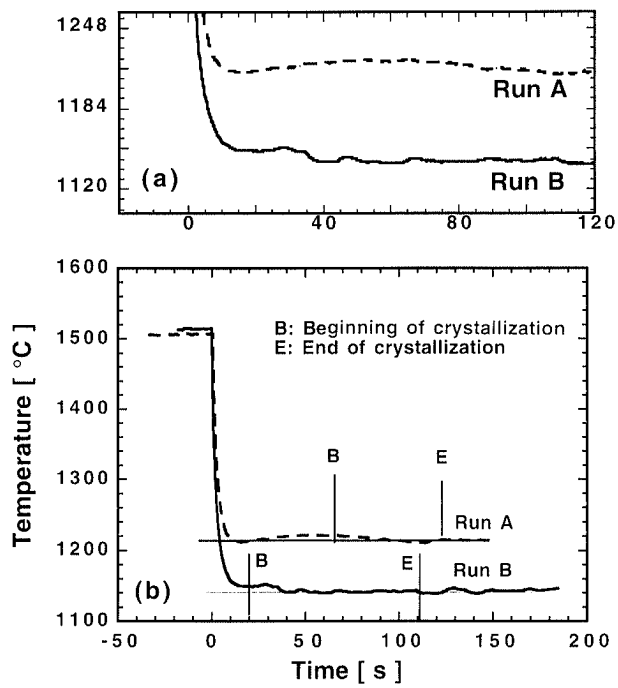

Fig. 2. Temperature variations of sample from quenching to steady state.

cases bubble formation was observed during the melting process.[29] The sample was held at 1 500°C for 4–5 min to eliminate the bubbles and homogenize its composition and temperature. After that, the sample was rapidly cooled to a given temperature and held for 5–60 min.

The sample images were recorded on a VCR and temperature–time curves were stored in a computer file. Image analysis of the video tape was used to determine the time for the beginning of crystallization and to measure the rate of crystal growth and the fraction of crystal transformed.

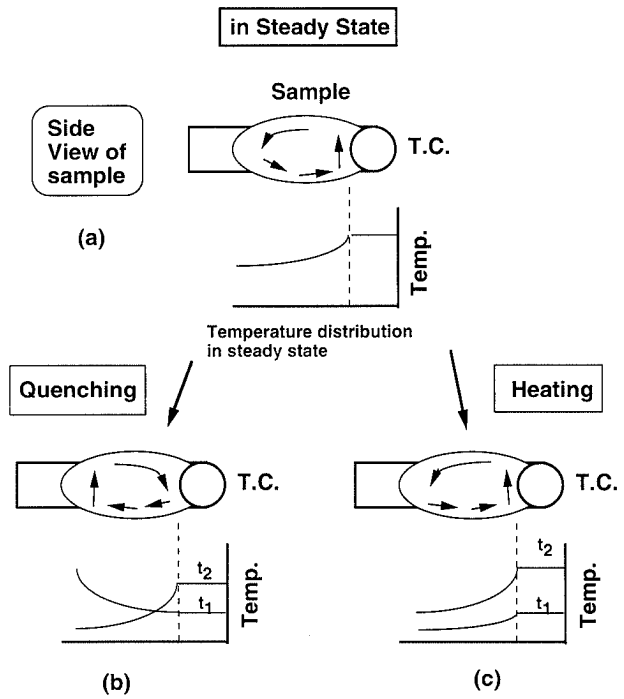

Fig. 3. Convection of sample in steady state and unsteady state during cooling and heating.

3. Results and Discussion

3.1. Temperature Profile and Convection in the Sample

Figure 2 shows the temperature profiles of experiments. In this experiment, the temperature was controlled by decreasing or increasing the electric current. Heat loss from the sample was by conduction to the thermocouple and by convection heat transfer to the ambient gases (air atmosphere). The profile of temperature in the sample should vary with the current; however there can be a time lag between the change in current and the attainment of isothermal conditions. Two cases are shown in Fig. 2(b). In Run A, at a higher testing temperature, a steady state is reached quickly and at the lower testing temperature (Run B) it takes longer to reach a steady state. Convection within the melt leads to temperature oscillations in the sample. Illustrations of convection in melt are shown in **Fig. 3** (side view of hot thermocouple). The detail of the hot thermocouple electrode in the top view was described in a previous paper.[29] At steady state, the sample temperature near the thermocouple is highest and there is a small temperature gradient from the tip of the thermocouple to the left hand side. The direction of the convection in steady state is shown in Fig.3 (a) (Due to the thermal gradient, Marangoni convection will dominate fluid flow in the system). When the sample was quenched, the temperature profile inside the sample would correspond to t_1 in Fig.

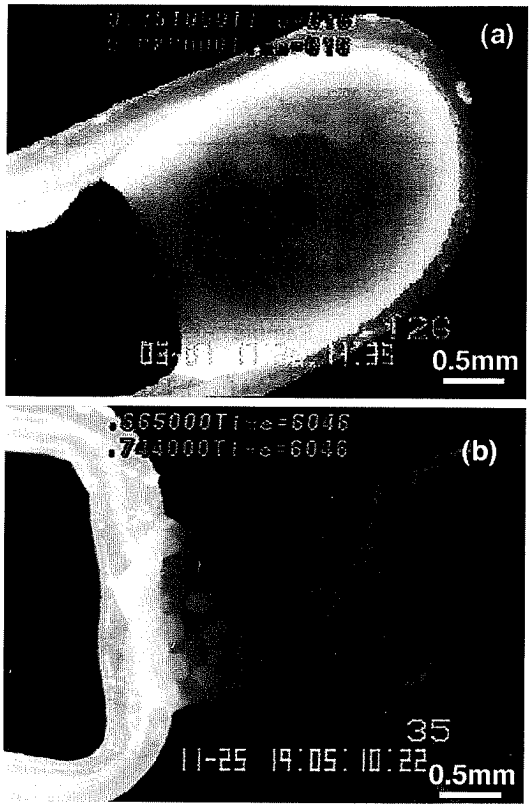

Fig. 4. Comparison of crystal image between simulated mold slag and industrial mold slag.

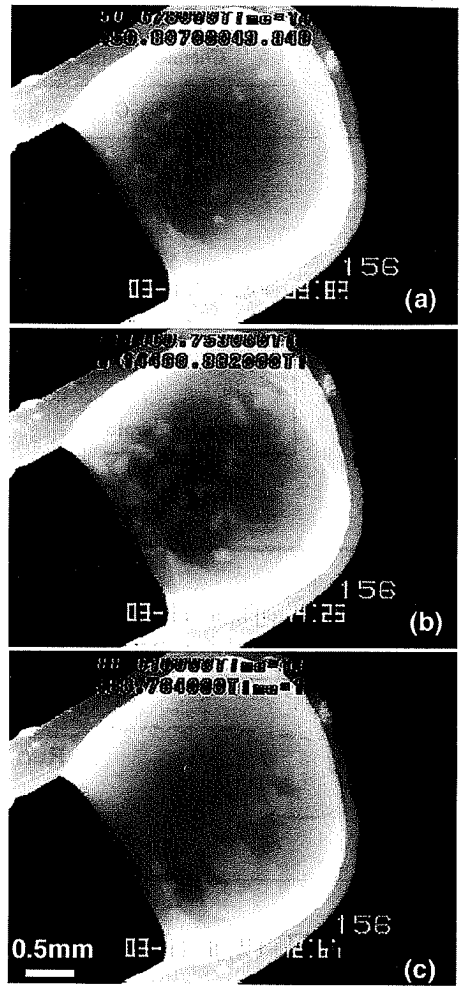

Fig. 5. Crystallization behavior of industrial mold slag. (1 142°C, Run B)

3(b) owing to the dominant heat conduction from the sample to the thermocouple. After that, the temperature profile will return to the steady state condition (t_2 or Fig. 3(a)). This phenomenon would correspond to the results of Run (A) and Run (B). In Run (A), since the temperature difference between testing temperature and melt temperature before quenching was smaller than that of Run (B), the time to return to steady state (from Fig. 3(b) to Fig. 3(a)) would be shorter than that of Run (B). Thus the direction of convection in sample B, at the beginning of crystallization, changed between Run (A) and Run (B). This change in convection direction in the sample has been confirmed by viewing the crystal movement, after precipitation, in the sample (Fig. 5 (Run B) and Fig.6 (Run A)). The crystals moved from the tip of thermocouple to the left hand side in the case of Run (A) in Fig.6. On the other hand, the crystals moved from the left hand side to the tip of thermocouple in Run (B) (Fig. 5).

Furthermore, as shown in Figs. 3(b) and 3(c), the direction of convection differed during quenching and heating. The convection in the sample was enhanced during heating, as the thermal gradient increased from the tip of thermocouple to the left hand side (Fig. 3(c)).

3.2. Results of *in Situ* Observation

Figure 4 shows the comparison of crystal image precipitated in the undercooled sample between an industrial mold slag (a) and a simulated mold slag (b), (3.8mass%Na_2O–6.8mass%Al_2O_3–44.7mass%SiO_2–44.7mass%CaO, C/S=1). Simulated mold slag experiments were carried out using the DHTT (Fig. 4(b)). For simulated slags the melt was transparent, the precipitated crystals were clearly visible and measurement of the number of nucleation events and the rate of crystal growth was unambiguous using automated computer image analysis. On the other hand, trials with an industrial mold slag revealed an image that was translucent (probably due to the iron oxide content of the flux) and more difficult to analyze by automated computer techniques (Fig. 4(a)).

In Fig. 4(a) crystallization in the industrial slag can be seen to occur by nucleation and growth of individual crystals in an undercooled liquid rather than by plane front solidification indicating that this phenomena must be treated using the techniques developed for classical nucleation theory. This industrial mold slag can undercool significantly below its equilibrium liquidus temperature and the phase diagram (if one existed) would not be useful in the determination of the conditions under which crystallization will occur. Additionally, this result suggests that nucleants could be used to modify the crystallization behavior of fluxes.

Figure 5 shows the sequence of crystal precipitation and growth in the sample at 1 142°C. The beginning of crystallization was 20 s from the start of cooling. Figs. 5(a), 5(b) and 5(c) were 16.32, 20.79 and 49.18 s from the beginning of crystallization, respectively. The crystals

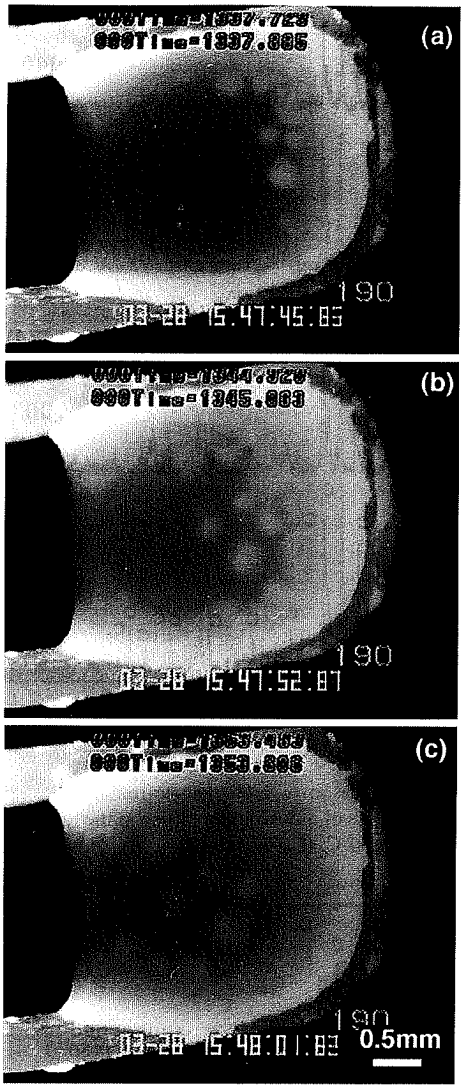

Fig. 6. Crystallization behavior of industrial mold slag. (1 215°C, Run A)

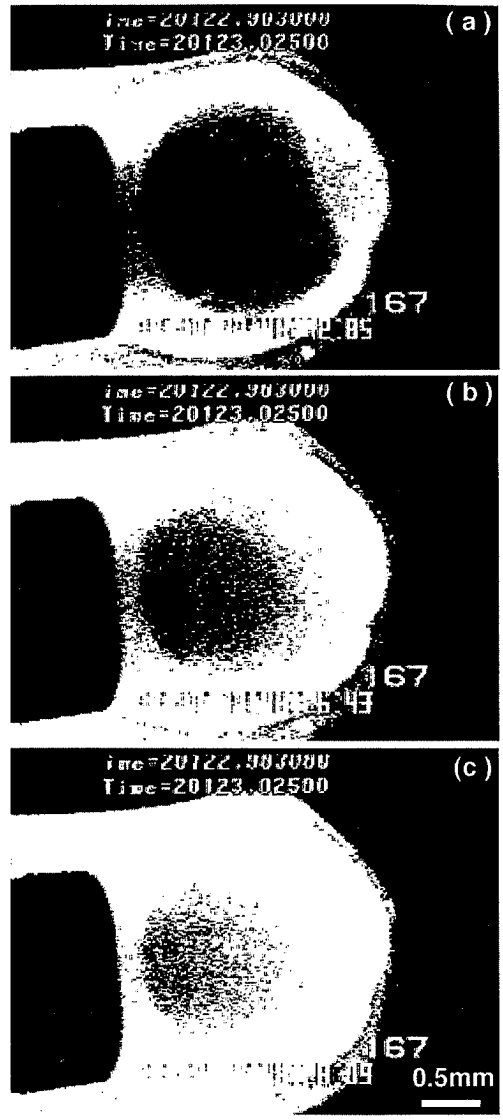

Fig. 7. Crystallization behavior of industrial mold slag. (1 009°C, Crystallized region was emphasized by image processing.)

began to appear from the left hand side of the sample, as mentioned before. Also it is interesting that the crystal morphology was not spherical but irregular and angular.

Figure 6 shows the sequence of crystallization at 1 215°C. The crystals were appeared spherical and the beginning of crystallization occurred 65 s after the start of the isothermal hold. Because of the long incubation time of crystallization, the convection in the sample had returned to a steady state (Fig. 3(a)) and the crystals began to be observed from the tip of thermocouple.

When the experimental temperature decreased to 1 009°C, the size of crystals were very small and it was difficult to measure the initial crystal size accurately (**Fig. 7**). To examine the morphology of the crystals, the sample was quenched from 1 200°C after crystallization had initiated. **Figure 8** shows the results of SEM observation. The crystals were dendrites even though a spherical crystal was observed macroscopically.

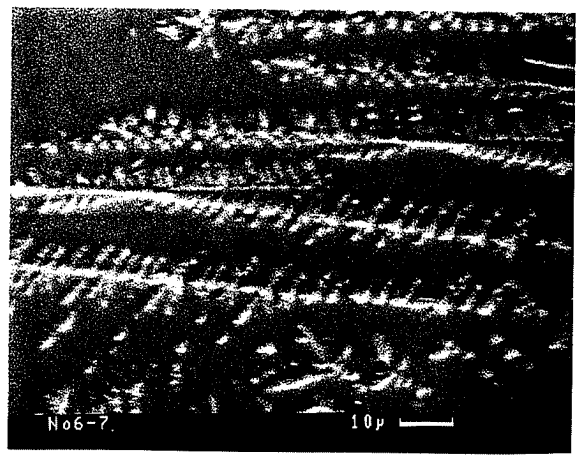

Fig. 8. SEM observation of crystallized part which sample was quenched from 1 200°C.

3.3. TTT Diagram and Mechanism of Crystal Growth

A number of experiments were performed over a wide range of temperatures in order to construct a TTT diagram for the mold flux using the SHTT. The beginning of crystallization which is defined when there is 0.5 vol% of crystallization, could be determined by image analysis ($t_{0.005}$) and the time of 50% volume fraction ($t_{0.5}$) were plotted against temperature and the TTT diagram ob-

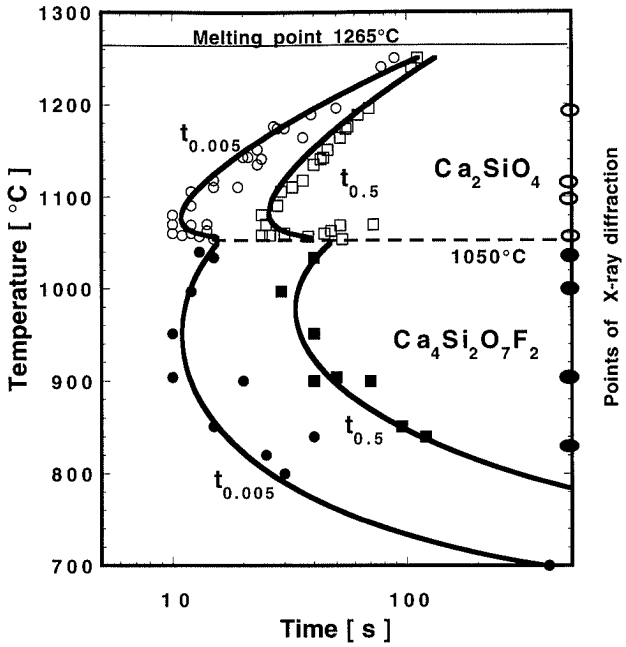

Fig. 9. TTT diagram of industrial mold slag obtained.

tained is shown in **Fig. 9**. The diagram was divided into two regions above and below 1 050°C as two distinct curves were detected which suggested two separate nucleation events. Each of the curves in the TTT diagram had a C-shape and the observed crystal morphology drastically changed at 1 050°C.

The minimum time before the crystalline phase could be determined was approximately 10 s at 1 070° and 950°C. The critical cooling rates for glass formation would be 30°C/s or higher for this industrial mold slag. The necessity of considering crystallization as function of time and temperature is clearly seen in Fig. 9. Also clear from this figure is that there is no specific crystallization temperature for a mold flux but a range of temperatures defined by experimental conditions.

To clarify the chemistry and structure of the crystal phase, X-ray diffraction of the sample were carried out using quenched samples and a high temperature X-ray diffraction technique. The maximum temperature of high temperature X-ray diffraction is 1 150°C and samples were prepared by quenching from 1 450°C. The sample was confirmed by ordinary X-ray diffraction as a totally amorphous phase before high temperature X-ray diffraction.

Figure 10 shows the high temperature X-ray diffraction patterns below 1 048°C. It was confirmed that the crystal phase below 1 048°C was Cuspidine ($Ca_4Si_2O_7F_2$, ASTM41-1474). The height of peaks decreased with increasing temperature, which means that the crystal became unstable close to 1 048°C.

Because of the upper temperature limit of the high temperature X-ray diffraction device, ordinary X-ray diffraction was carried out to characterize the higher temperature phases using quenched samples which were melted on the hot thermocouple at each temperature, held until crystallization finished and then quenched by a gas jet (cooling rate ≈150°C/s). **Figure 11** shows the comparison of X-ray diffraction patterns between high

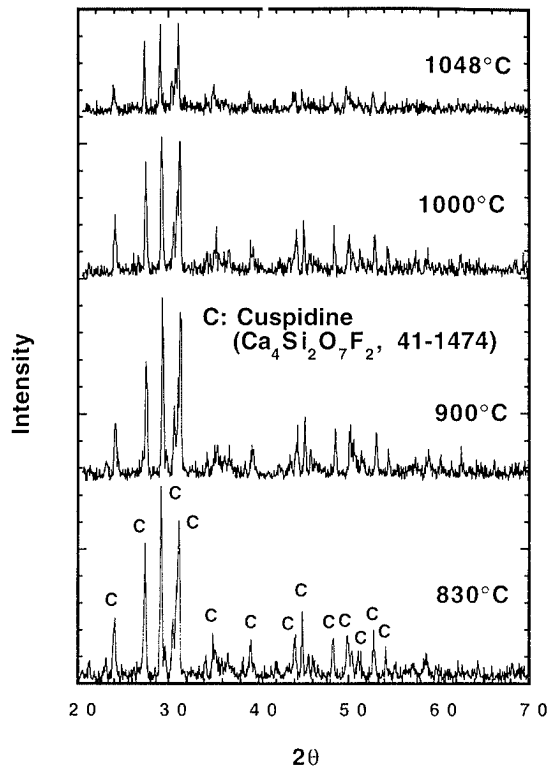

Fig. 10. Comparison of high temperature X-ray diffraction patterns of industrial mold slag in the range from 830 to 1 050°C. (Cu-$K\alpha$)

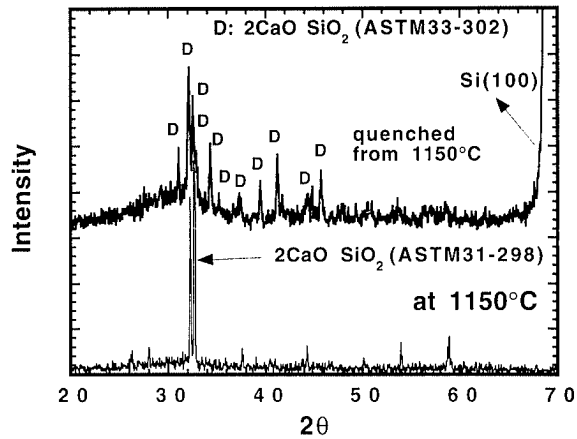

Fig. 11. X-ray diffraction patterns between quenched sample and sample at high temperature. (Cu-$K\alpha$)

temperature X-ray diffraction at 1 150°C and ordinary X-ray diffraction of sample quenched from 1 150°C. It was found that the phase was $2CaO \cdot SiO_2$ in both cases.

Figure 12 shows the X-ray diffraction patterns of samples quenched from 1 053° to 1 190°C using the SHTT. Dicalcium silicate (Ca_2SiO_4) was the dominant phase measured in this temperature range. These X-ray diffraction results (Figs. 10 and 12) allow the two curves in the TTT diagram to be identified.

3.4. Kinetics of Crystal Growth in High Temperature Region

Image analyses were performed to obtain the rate of crystal growth and to evaluate the volume fraction of crystals evolved as a function of time. As mentioned before, the crystal image was not as clear as a simulated

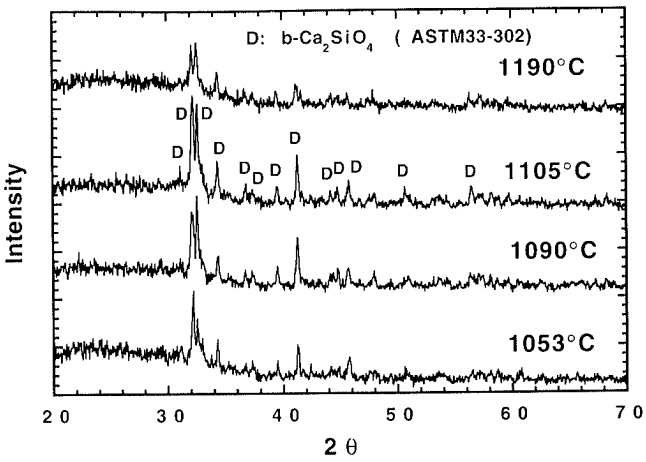

Fig. 12. Comparison of X-ray diffraction patterns of industrial mold slag from 1 053 to 1 190°C. (Cu-$K\alpha$)

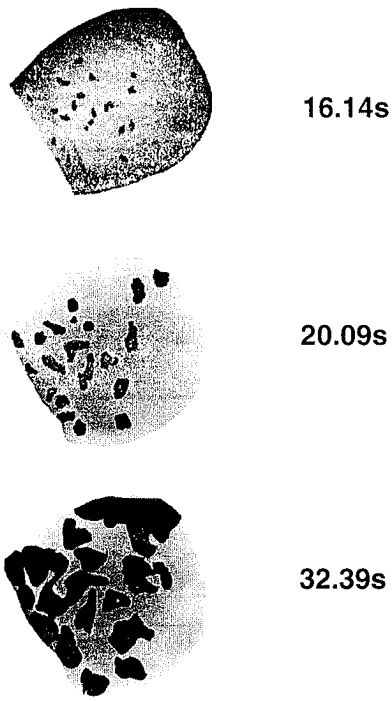

Fig. 13. Variation of crystallized area in industrial mold slag. (1 142°C, Run B)

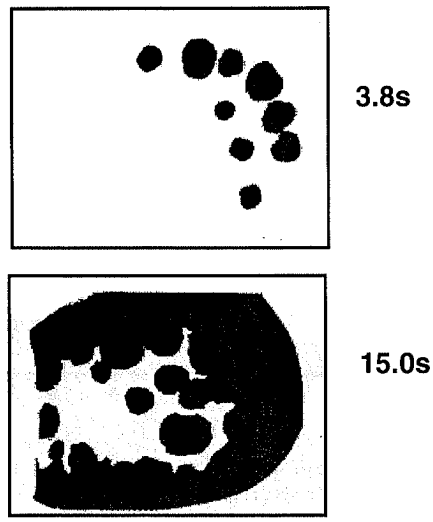

Fig. 14. Variation of crystallized area in industrial mold slag. (1 215°C, Run A)

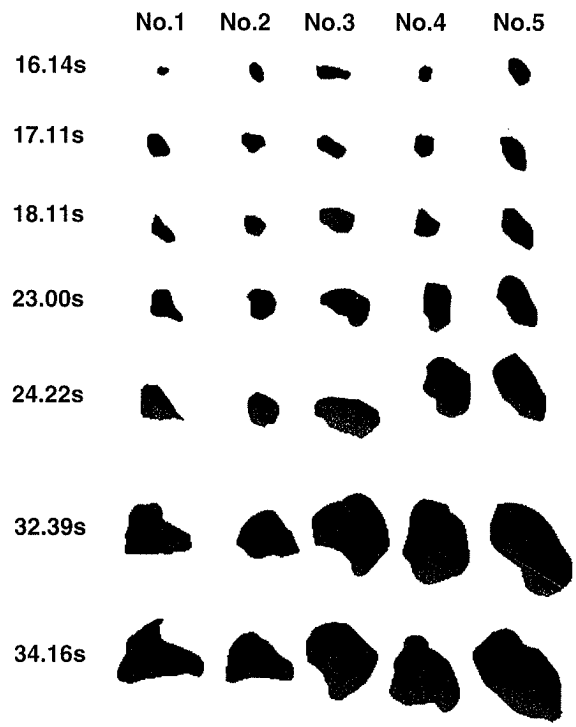

Fig. 15. Variation of crystal size precipitated in sample. (1 142°C, Run B)

mold slag which made automatic image analysis difficult as computerized edge detection was not possible. The portion of crystals which could be clearly recognized were outlined in each frame manually and their areas were counted by computer (**Figs. 13** and **14**). The particles were treated as spherical in cross-section and the volume was calculated using the thickness of the sample. Although the detail of crystal outline could not reproduced exactly, a total of 200 000 pixels were used for calculation and the error was within 5% for several calculations. Also each of the crystals were extracted and volumes were calculated from the area ($V=4/3\cdot\pi(A/\pi)^{3/2}$, V: cm^3, A: cm^2) and results are shown in **Fig. 15**. The variation of crystal volume fraction with time was compared with the volume fraction of the crystal in the whole sample in **Fig. 16**. In each method, the variation of volume fractions $F(t)$ was the same and could be represented by Avrami Equation.[32-42]

$$F(t)=1-\exp(-(K\cdot t)^n) \quad \text{.....(1)}$$

where n represents the mechanism of crystal growth and K is a coefficient corresponding to the nucleation and growth mechanism. For a constant volume nucleation rate N, n is equal to 4 and the equation is equal to Johnson–Mehl–Avrami equation.[32]

$$F(t)=1-\exp(-(\pi\cdot N\cdot u^3/3)\cdot t^4) \quad \text{.....(2)}$$

where u is growth rate. The value of n which is equal to 4 means that the rate of reaction is quite fast and a non-diffusional transport mechanism is dominant. This transport mechanism of the crystal growth in an industrial mold slag during the experiment is probably due to convection.

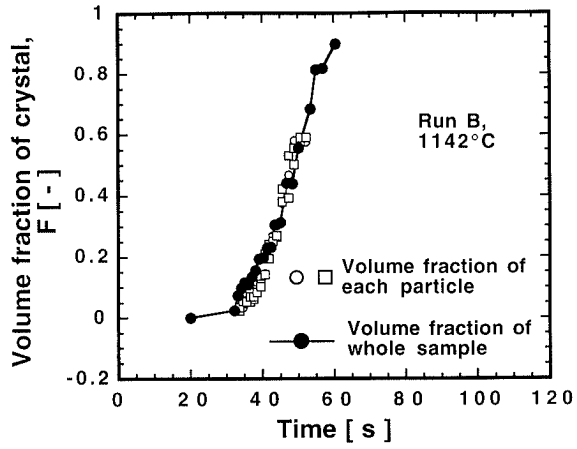

Fig. 16. Comparison of variation of volume fraction between whole sample and each particles.

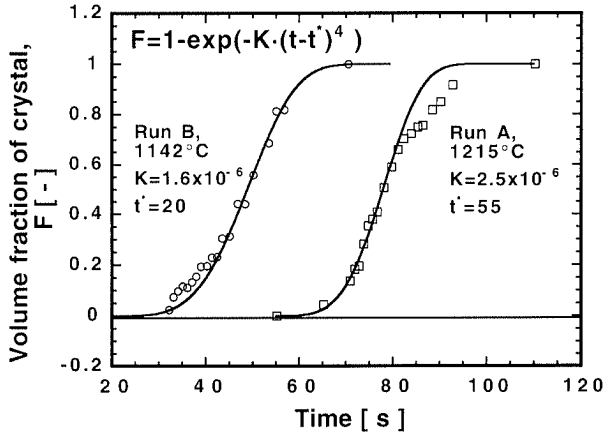

Fig. 17. Comparison of volume fractions of crystal between observations and calculation.

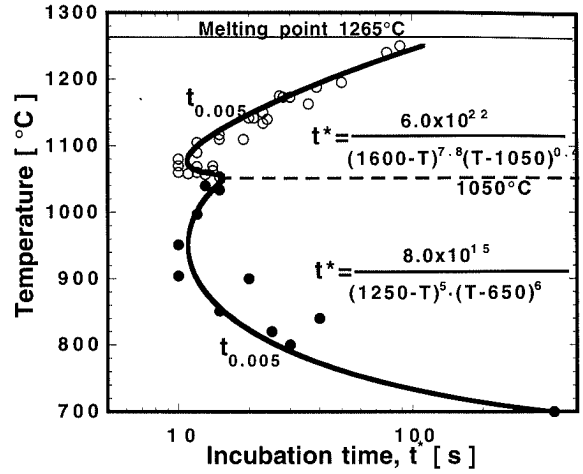

Fig. 18. Comparison of calculated incubation time with estimated one from $t_{0.005}$ and $t_{0.5}$.

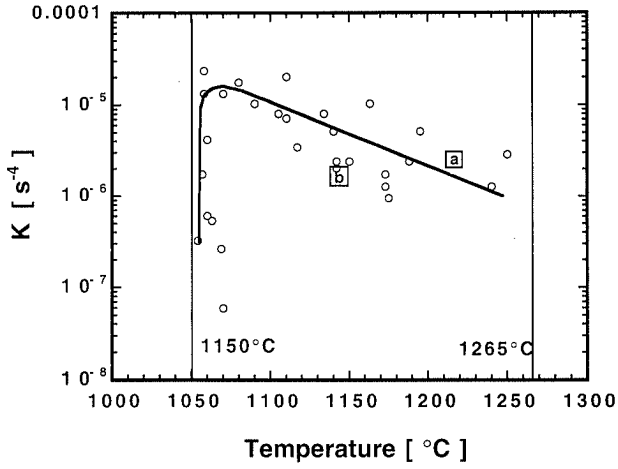

Fig. 19. Variation of coefficient K in Avrami Eq. for crystal growth of industrial mold slag.

Figure 17 shows a comparison of calculated and observed crystal growth rate at 1 215 and 1 142°C. The calculation of crystal growth rate at 1 215°C was in good agreement with the observation until 70 % of the volume had transformed. However, because of temperature decrease (Fig. 2 Run A), the rate of crystal growth was retarded at this time. In the case of 1 142°C, the temperature in the initial stage of crystal growth (<45 s, Fig. 2) was higher (≈1 150°C) than the average temperature, so that the deviation of measured crystal growth was observed in the upper side of the calculation. As shown in Fig. 9, the observed results had relatively large scatter, since the nucleation and growth in each experiment was strongly affected by temperature and the number of nucleation sites in the sample. The surface of a liquid often provides a nucleation site; however in this study, the crystal appeared inside the sample. Occasionally it was observed that the crystal grew from a small bubble that remained in the sample.

If the nucleation rate is zero before a given incubation time t^*, Eq. (2) can be modified to Eq. (3).

$$F(t)=1-\exp(-K\cdot(t-t^*)^4) \quad \text{.....(3)}$$

The incubation time (t^*) and coefficient K were calculated from the mean values measured in each experiment. Using time at 0.05 and 50 % volume fraction, $t_{0.005}$ and $t_{0.5}$, the following expression is obtained from Eq. (3).

$$\varphi=\left[\frac{\ln(1-0.005)}{\ln(1-0.5)}\right]^{1/4}=\frac{t_{0.005}-t^*}{t_{0.5}-t^*} \quad \text{.....(4)}$$

Then incubation times t^* were obtained for each experiment and plotted in **Fig. 18** for each temperature ranges.

$$t^*=\frac{\varphi\cdot t_{0.5}-t_{0.005}}{\varphi-1} \quad \text{.....(5)}$$

It is useful to use an empirical expression for describing the incubation time as a function of temperature. The following expressions give acceptable calculation results that fit the measured incubation time.

$$t^*=\frac{6.0\times10^{22}}{(1\,600-T)^{7.8}(T-1\,050)^{0.4}}$$
$$1\,050°C<T<1\,265°C$$

$$t^*=\frac{8.0\times10^{15}}{(1\,250-T)^{3.0}(T-650)^{3.0}}$$
$$700°C<T<1\,050°C$$

The coefficients K in each experiment were calculated from the incubation time t^* and Eq. (3) and are shown

in **Fig. 19**. As mentioned before, nucleation and crystal growth are strongly affected by temperature and the number of nucleation sites in each experiment and the derived coefficient K has a relatively large scatter. The coefficients K obtained at 1 215 and 1 142°C by fitting to the Eq. (3) were 2.5×10^{-6} to 1.6×10^{-6}, respectively, and are plotted in Fig. 19 as the points marked as 'a' and 'b'. Although the coefficients K in 1 215 and 1 142°C were within the region of error in Fig.18, the values could not be predicted from the average value.

4. Conclusions

The Single Hot Thermocouple Technique (SHTT) was employed to study the crystallization behavior of an industrial mold slag. This technique proved to be effective to visualize the beginning of crystallization and to measure the variation of the crystals size and volume fraction as a function of time. Isothermal tests were carried out at different temperatures and a TTT diagram for an industrial mold slag was determined. The TTT diagram was divided into two regions above and below 1 050°C as two different phases were seen to nucleate and grow in these different temperature regimes. The crystal phases were determined by X-ray diffraction of the sample and dicalcium silicate (Ca_2SiO_4) and cuspidine ($Ca_4Si_2O_7F_2$) corresponded to high temperature and low temperature region of the TTT diagram, respectively.

The Avrami equation was applied for the crystal growth at high temperature and Johnson–Mehl–Avrami type equation was found to represent the observed results for crystal growth at temperatures over 1 050°C.

Acknowledgement

This research was funded by the Center for Iron and Steelmaking Research at Carnegie Mellon University.

REFERENCES

1) M. Wolf: ISS Process Technology Conf., 13, (1995), 99.
2) K. Mills, P. Grievson, A. Osuanya and S. Bacha: TIM–Continuous Casting, (1985), 571.
3) K. Mills: ISS Steelmaking Proc., (1991), 121.
4) M. Jenkins: ISS Steelmaking Proc., (1995), 315.
5) A. Yamauchi, K. Sorimachi, T. Sakuraya and T. Fuji: *ISIJ Int.*, **33** (1993), 140.
6) M. Susa, K. Mills, M. Richardson, R. Taylor and D. Stewart: *Ironmaking Steelmaking*, **21** (1994), 279.
7) M. Emi: ISS Steelmaking Proc., (1991), 623.
8) H. Kyoden, T. Doihara and O. Nomura: ISS Steelmaking Proc., (1986), 153.
9) T. Wada, M. Suzuki and T. Mori: *Iron Steelmaker*, (1987), 31.
10) T. Kappey: ISS Steelmaking Proc., (1992), 543.
11) H. Gilles, M. Byrne, T. Ruso and G. DeMasi: ISS Process Technology Conf. Proc., (1990), 123.
12) K. Sorimachi, M. Kuga, M. Saigusa and T. Sakuraya: *Fachber. Hütttenprax. Metallweiterverarb.*, **20** (1982), 244.
13) H. Nakato, T. Sakuraya, T. Nozaki, T. Emi and H. Nishikawa: ISS Steelmaking Proc., (1986), 137.
14) M. Frazee: ISS Steelmaking Proc., (1995), 639.
15) R. Branion, D. Dukelow, G. Lawson, J. Schade, M. Schmidt and H. Tsai: ISS Steelmaking Proc., (1995), 647.
16) T. Kishi, H. Tsuboi, H. Takeuchi, T. Nakano, M. Yamamiya and T. Ando: *Nippon Steel Tech. Rep.*, **34** (1987), 11.
17) R. Bommaraju: ISS Steelmaking Proc., (1991), 131.
18) H. Sakai, T. Kawashima, T. Shiomi, K. Watanabe and T. Iida: Molten Slags, Fluxes and Salts '97 Conf., (1997), 787.
19) K. Watanabe, M. Suzuki, K. Murakami, H. Kondo, A. Miyamoto and T. Shiomi: *Tetsu-to-Hagané*, **83** (1997), 31.
20) G. Fisher, A. Golloch and J. Kasajanow: *Steel Res.*, **67** (1996), 479.
21) J. Chávez, A. Rodríguez, R. Morales and V. Tapia: ISS Steelmaking Proc., (1995), 679.
22) M. Bhamra, M. Charlesworth, S. Wong, D. Sawyers-Villers and A. Cramb: ISS Electric Furnace Conf., (1996), 551.
23) J. Dubrawski and J. Camplin: *J. Therm. Anal.*, **40** (1993), 329.
24) O. Afrange, M. Fonseca and H. Polivanov: Conf. on Continuous Casting of Steel in Developing Countries, China, (1993), 623.
25) P. Hammerschmid and D. Janke: *Steel Res.*, **9** (1991), 395.
26) M. Lanyi and C. Rosa: *Metall. Trans. B*, **12** (1981), 287.
27) S. Chang, I. Lee, M. Kim, S. Yang, J. Choic and J. Park: Conf. on Continuous Casting of Steel in Developing Countries, China, (1993), 832.
28) W. Qiang, X. Bing and C. Jinghao: Conf. on Continuous Casting of Steel in Developing Countries, China, (1993), 842.
29) Y. Kashiwaya, C.E. Cicutti, A. Cramb and K. Ishii: *ISIJ Int.*, **38** (1998), 348.
30) D. Uhlman: *J. Am. Ceram. Soc.*, **66** (1983), 95.
31) C. Gatellier, H. Gaye, J. Lehmann, J. Pontoire and P. Riboud: *Steel Res.*, **64** (1993), 87.
32) K. F. Kelton: Solid State Physics, Vol. 45, Crystal Nucleation in Liquids and Glasses, Academic Press, Inc., New York, (1991), 75.
33) M. Avrami: *J. Chem. Phys.*, **7** (1939), 1103.
34) W. A. Johnson and R. F. Mehl: *TAIME*, **135** (1939), 416.
35) H. Rawson: Inorganic Glass-Forming System, Academic Press, London, (1967), 160.
36) G. Lucadamo, K. Barmak and C. Michaelsen: *Mat. Res. Soc. Symp. Proc.*, **398** (1996), 227.
37) J. W. Cahn: *Mat. Res. Soc. Symp. Proc.*, **398** (1996), 425.
38) P.G. Shewmon: Transformation in Metals., McGraw-Hill, New York, (1969), 88.
39) J. Jean and T. K. Gupta: Kinetic of Cristobalite Formation Binary Borosilicate High Silica Glass Composite, Ceramic Transactions, Vol. 30, (1992), Nucleation and Crystallization in Glasses and Liquids, 347.
40) R. Hill: Physical Metallurgy Principles, D. Van Nostrand Co., (1960), 447.
41) A. Navrotsky: *Met. Res. Soc. Symp. Proc.*, **321** (1994), 3.